

thiolate substituents effectively block further secondary interactions or of some more subtle steric or electronic effects remains problematical.

Acknowledgment. We gratefully acknowledge support from the National Science Foundation, the National Institutes of Health, the donors of the Petroleum Research Fund, administered by the American Chemical Society, the Herman Frasch Foundation, and Société Nationale Elf Aquitaine. Funding for the 300-MHz NMR facility was provided by the National Science

Foundation.

Supplementary Material Available: Tables of bond lengths (Tables S1 and S10), bond angles, (Tables S2 and S11), anisotropic temperature factors (Tables S3 and S12), and calculated hydrogen atom positions (Tables S4 and S13) for I and III, tables of bond lengths (Table S6), bond angles (Table S7), and anisotropic temperature factors (Table S8) for II, and a summary of the experimental details for the X-ray diffraction studies of I-III (Table S15) (22 pages); tables of observed and calculated structure factors (Tables S5, S9, and S14) for I-III (65 pages). Ordering information is given on any current masthead page.

Contribution from the Research School of Chemistry, Australian National University, GPO Box 4, Canberra, ACT 2601, Australia, Chemistry Department, University of Tasmania, GPO Box 252C, Hobart, Tasmania 7001, Australia, and Division of Mineral Products, CSIRO, PO Box 124, Port Melbourne, Victoria 3207, Australia

Magneto-Structural Correlations and Metal-Metal Bonding in Exchange-Coupled

$A_3Mo_2X_9$ ($X = Cl, Br, I$) Complexes

Robert Stranger,^{*,†} Peter W. Smith,[‡] and Ian E. Grey[§]

Received June 13, 1988

The magneto-structural properties and the role of M-M bonding in $A_3Mo_2X_9$ ($X = Cl, Br, I$) complexes are examined. Structural and magnetic data are given for the new salts $A_3Mo_2X_9$ [$A = Rb, NH_4, RNH_3$ ($R = Me, Et, Bu, Hex$), R_2NH_2 ($R = Me, Et$), Me_3NH], $A_3Mo_2Br_9$ ($A = Rb, Me_4N$), and $A_3Mo_2I_9$ ($A = Cs, EtNH_3$). The structure of $(MeNH_3)_3Mo_2Cl_9$ was refined by Rietveld analysis of powder X-ray diffraction data. It has orthorhombic symmetry, space group $Cmcm$ ($Z = 4$), with unit cell dimensions of $a = 7.187$ (1) Å, $b = 15.086$ (1) Å, and $c = 17.649$ (1) Å. The $MeNH_3$ group is oriented along the b axis, and the geometry of the $Mo_2Cl_9^{3-}$ anion is almost identical with that in $Cs_3Mo_2Cl_9$. The cation effect on the M_2X_9 structure is shown to result from a size increase along the c axis direction of the A(1) cation lying in the plane of the bridging halogens. For the strongly coupled $Mo_2X_9^{3-}$ anion, calculations show that the ground-pair levels no longer obey a Heisenberg (HDVV) coupling although the $S = 0, 1, 2$ pair spin levels still follow a Landé type interval separation. The ground exchange coupling is shown to be very sensitive to the single-ion electron repulsion parameters, and the weakly coupled limit applies only when the single-ion Coulombic exchange is at least 5 times greater than the largest pair-exchange parameter. The observed correlation between J_{ab} and the M-M separation in $A_3Mo_2Cl_9$ complexes is modeled by using a semiquantitative MO model based on the M-M σ -orbital overlap.

Introduction

The complex salts of stoichiometry $A_3M_2X_9$ represent an ideal series to study magneto-structural correlations in exchange-coupled systems since variation in A, M, or X can significantly alter the observed magnetic and spectroscopic properties of the $M_2X_9^{3-}$ binuclear unit. Studies on a number of such systems containing paramagnetic M^{3+} transition-metal ions have appeared previously in the literature.¹⁻³⁸ Intermediate between the weakly coupled $Cr_2X_9^{3-}$ and metal-metal-bonded $W_2X_9^{3-}$ anions are the complex salts of $Mo_2X_9^{3-}$. Magnetic studies on this system³⁶⁻³⁹ have shown the ground exchange coupling to be strongly antiferromagnetic and quite sensitive to the size of the univalent A cation.^{36,37} An exponential relationship between the ground magnetic exchange constant J_{ab} and the M-M separation in the binuclear unit was obtained in the case of spherical A cations. The metal-metal distances used were derived from the c axis unit cell lengths on the assumption of a constant z/c fractional coordinate for the Mo atoms. However, we recently reported³⁵ structural refinements using the Rietveld method⁴⁰ on a number of alkali-metal and alkylammonium salts of $Mo_2X_9^{3-}$ ($X = Cl, Br, I$). The previous assumption of a constant z/c fractional coordinate for Mo was not observed, particularly for the alkylammonium salts. Furthermore, magnetic studies on a number of substituted pyridinium and piperidinium salts of $Mo_2X_9^{3-}$ ($X = Cl, Br$) have since been reported³⁸ and these salts deviate significantly from the above J_{ab} versus M-M separation curve. Finally, previous magnetic studies³⁶⁻³⁹ have ignored the effects of M-M bonding on the ground exchange coupling, yet the electronic spectrum of $Cs_3Mo_2Cl_9$ has now been interpreted on

the basis of a large M-M σ interaction and two weaker π interactions.⁴³

- (1) Wessel, G. J.; Idjo, D. J. W. *Acta Crystallogr.* 1957, 10, 466.
- (2) Idjo, D. J. W. Ph.D. Thesis, Leiden, 1960.
- (3) Earnshaw, A.; Lewis, J. J. *J. Chem. Soc.* 1961, 396.
- (4) Saillant, R.; Wentworth, R. A. D. *Inorg. Chem.* 1968, 7, 1606.
- (5) Grey, I. E.; Smith, P. W. *Aust. J. Chem.* 1971, 24, 73.
- (6) Beswick, J. R.; Dugdale, D. E. *J. Phys. C* 1973, 6, 3326.
- (7) Kahn, O.; Briat, B. *Chem. Phys. Lett.* 1975, 32, 376.
- (8) Dubicki, L.; Ferguson, J.; Harrowfield, B. *Mol. Phys.* 1977, 34, 1545.
- (9) Briat, B.; Russel, M. F.; Rivoal, J. C.; Chapelle, J. P.; Kahn, O. *Mol. Phys.* 1977, 34, 1357.
- (10) Johnstone, I. W.; Briat, B.; Lockwood, D. J. *Solid State Commun.* 1980, 35B, 689.
- (11) Johnstone, I. W.; Maxwell, K. J.; Stevens, K. W. H. *J. Phys. C* 1981, 14, 1297.
- (12) Dean, N. J.; Maxwell, K. J. *Mol. Phys.* 1982, 47, 551.
- (13) Leuenberger, B.; Güdel, H. U.; Feile, R.; Kjems, K. J. *Phys. Rev. B* 1983, 28, 5368.
- (14) Leuenberger, B.; Stebler, A.; Güdel, H. U.; Furrer, A.; Feile, R.; Kjems, J. K. *Phys. Rev. B* 1984, 30, 6300.
- (15) Leuenberger, B.; Güdel, H. U.; Kjems, J. K. *J. Magn. Magn. Mater.* 1985, 53, 175.
- (16) Leuenberger, B.; Güdel, H. U.; Fischer, P. *Phys. Rev. Lett.* 1985, 55, 2983.
- (17) Leuenberger, B.; Güdel, H. U.; Kjems, J. K.; Petitgrand, D. *Inorg. Chem.* 1985, 24, 1035.
- (18) Dean, N. J.; Maxwell, K. J.; Stevens, K. W. H.; Turner, R. J. *J. Phys. C* 1985, 18, 4505.
- (19) Leuenberger, B.; Güdel, H. U.; Fischer, P. *Phys. Rev. B* 1986, 33, 6375.
- (20) Güdel, H. U.; Furrer, A.; Kjems, J. K. *J. Magn. Magn. Mater.* 1986, 54, 1453.
- (21) Leuenberger, B.; Güdel, H. U.; Fischer, P. *J. Solid State Chem.* 1986, 64, 90.
- (22) Dean, N. J.; Maxwell, K. J. *Chem. Phys.* 1986, 106, 233.
- (23) Leuenberger, B.; Güdel, H. U. *Inorg. Chem.* 1986, 25, 181.
- (24) Leuenberger, B. *Mol. Phys.* 1986, 59, 249.
- (25) Fowles, G. W. A.; Russ, B. J. *J. Chem. Soc. A* 1967, 517.
- (26) Crough, P. C.; Fowles, G. W. A.; Walton, R. A. *J. Chem. Soc. A* 1967, 972.
- (27) Barraclough, C. R.; Gregson, A. K. *J. Chem. Soc. Faraday Trans.* 1972, 2, 177.

* To whom correspondence should be addressed.

† Australian National University.

‡ University of Tasmania.

§ CSIRO.

In light of the above, the influence of the A cation on the structural and magnetic properties of $\text{Mo}_2\text{X}_9^{3-}$ salts needs to be rationalized and the relationship between the M-M separation and J_{ab} determined over a range of $\text{A}_3\text{Mo}_2\text{X}_9$ complexes. In addition, the effect of M-M bonding on the ground exchange coupling should be examined in order to assess the validity of a simple Heisenberg-Dirac-Van Vleck (HDVV) description of the ground state.

Experimental Section

Preparations. The alkylammonium salts of $\text{Mo}_2\text{Cl}_9^{3-}$ were prepared by solution methods previously reported.^{36,37} The alkali-metal and ammonium salts were prepared in a similar manner with the exception that the cation was added as its acetate salt in order to afford solubility in alcoholic solutions. The corresponding bromide and iodide complexes were prepared by repeated additions of HBr or HI, followed by concentration, to the original Mo(III)-acid chloride solution.^{39,42}

Structural Measurements. The X-ray powder diffraction data for $(\text{MeNH}_3)_3\text{Mo}_2\text{Cl}_9$ were collected by using a Philips PW1050 goniometer fitted with a PW1710 controller. Intensity measurements in the range $7-90^\circ$ (2θ) were made at intervals of 0.04° (2θ) by using $\text{Cu K}\alpha$ radiation and a step-counting time of 5 s. The X-ray tube was operated at 45 kV and 30 mA, with 1° divergence slit, a 0.2-mm receiving slit, and a 1° scatter slit and Soller slits. For angles less than 14° (2θ) a geometrical correction was made for the spread of the beam beyond the sample. The structure refinement of $(\text{MeNH}_3)_3\text{Mo}_2\text{Cl}_9$ was carried out by using a modified version⁵⁸ of the Rietveld Profile Analysis program *DPW3.2*.⁴⁰ Starting coordinates for the Mo and Cl atoms in *Cmcm* were those obtained from a single-crystal refinement for the isostructural ethylammonium salt.⁴⁶ The N and C atoms were located in difference Fourier maps. The final refinement utilized data in the range $16-90^\circ$ (2θ), and 36 parameters were refined, including 16 coordinates, 5 isotropic temperature factors, and 15 profile and unit cell parameters. Profile refinement parameters used have been described previously.³⁵ Neutral-atom X-ray scattering factors, including anomalous dispersion corrections, were taken from ref 56.

Magnetic Measurements. Magnetic susceptibilities were measured on powdered samples by the Guoy method between 80 and 450 K. The magnetic field was calibrated by using $\text{CuSO}_4 \cdot 5\text{H}_2\text{O}$ packed in a silica Guoy tube that had a constant diamagnetic correction over the temper-

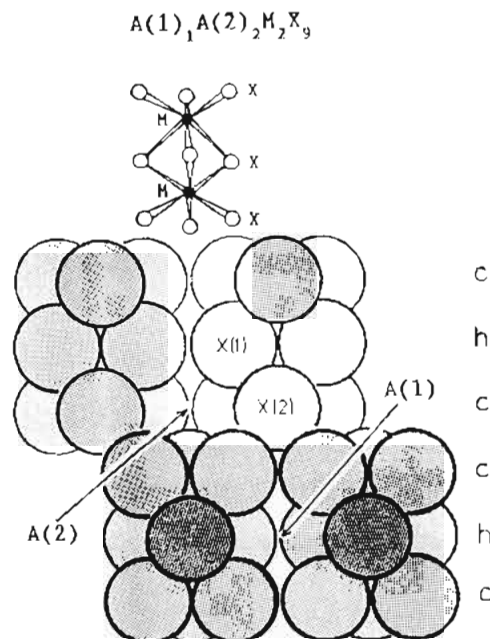


Figure 1. Close-packing arrangement in $\text{A}_3\text{M}_2\text{X}_9$ complexes viewed along $[11,2,0]$. The bridging X(1) and terminal X(2) halogens occupy hexagonal (h) and cubic (c) layers, respectively. The A(1) and A(2) cation sites are shown. Metal ions M occupy two-thirds of the octahedral sites between h and c layers.

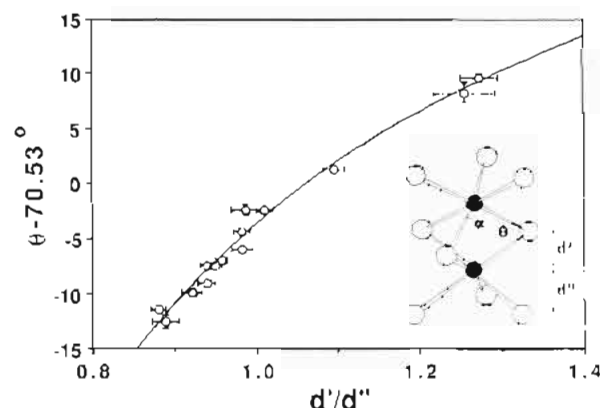


Figure 2. Correlation between structural moduli in $\text{A}_3\text{M}_2\text{X}_9$ complexes. The parameters d' and d'' correspond to the M-h and M-c layer separations, while the parameters α and θ are the X(1)-M-X(1) and M-X(1)-M bridging angles. The ratio d'/d'' measures the displacement of the metal ions M from the centroids of their octahedra, while $\theta - 70.53$ measures the deviation of the M-X(1)-M bridging angle from the ideal value of 70.53° for two octahedra sharing a common trigonal face. The X(1)-M-X(1) bridging angle α is related to θ through the expression $\sin(\alpha/2) = (\sqrt{3}/2) \cos(\theta/2)$. In order of increasing d'/d'' , the experimental points correspond to $\text{K}_3\text{Mo}_2\text{Br}_9$, $\text{K}_3\text{W}_2\text{Cl}_9$, $\text{Cs}_3\text{W}_2\text{Cl}_9$, $\text{Rb}_3\text{Mo}_2\text{Br}_9$, $\text{Rb}_3\text{Mo}_2\text{Cl}_9$, $(\text{NH}_4)_3\text{Mo}_2\text{Cl}_9$, $\text{Cs}_3\text{Mo}_2\text{Br}_9$, $\text{Cs}_3\text{Mo}_2\text{Cl}_9$, $\text{Cs}_3\text{Mo}_2\text{I}_9$, $(\text{Me}_4\text{N})_3\text{Mo}_2\text{Cl}_9$, $(\text{Me}_4\text{N})_3\text{Mo}_2\text{Br}_9$, $\text{Cs}_3\text{Cr}_2\text{Cl}_9$, and $\text{Cs}_3\text{Cr}_2\text{Br}_9$.

ature range studied. Diamagnetic corrections for cation A and halogen X were made in accordance with standard values.⁵⁷ ESR measurements were carried out on powdered samples at room temperature by using a Jeol FE3X ESR spectrometer.

Results

Structures Containing Symmetric Cations. The complex salts $\text{A}_3\text{Mo}_2\text{X}_9$ ($\text{A} = \text{K}, \text{Rb}, \text{NH}_4, \text{Cs}, \text{Me}_4\text{N}, \text{Et}_4\text{N}$; $\text{X} = \text{Cl}, \text{Br}, \text{I}$) containing spherical or pseudospherical univalent cations A crystallize in either $P6_3/mmc$ or $P6_3/m$ ($Z = 2$) hexagonal space groups.^{35,41,42} In either case, the structure can be described in terms of a close-packing arrangement of (0001) layers of composition

- (28) Briat, B.; Kahn, O.; Morgenstern-Badarau, I.; Rivoal, J. C. *Inorg. Chem.* **1981**, *20*, 4193.
 (29) Leuenberger, B.; Güdel, H. U.; Furrer, A. *Chem. Phys. Lett.* **1986**, *126*, 255.
 (30) Leuenberger, B.; Briat, B.; Canit, J. C.; Furrer, A.; Fischer, P.; Güdel, H. U. *Inorg. Chem.* **1986**, *25*, 2930.
 (31) Drillon, M.; Georges, R. *Phys. Rev. B* **1982**, *26*, 3882.
 (32) Leuenberger, B.; Güdel, H. U. *Mol. Phys.* **1984**, *51*, 1.
 (33) Leuenberger, B. *Mol. Phys.* **1986**, *59*, 2.
 (34) Watson, W. H.; Waser, J. *Acta Crystallogr.* **1958**, *11*, 689.
 (35) Stranger, R.; Grey, I. E.; Madsen, I. C.; Smith, P. W. *J. Solid State Chem.* **1987**, *69*, 162.
 (36) Grey, I. E.; Smith, P. W. *Aust. J. Chem.* **1969**, *22*, 121.
 (37) Grey, I. E.; Smith, P. W. *Aust. J. Chem.* **1971**, *24*, 73.
 (38) Zelentsov, V. V.; Hguen Hui Chi; Fal'kengof, A. T.; Subbotina, N. A.; Spitsyn, V. I. *Russ. J. Inorg. Chem. (Engl. Transl.)* **1973**, *18*, 1483.
 (39) Gregg, G. C. Honours Thesis, University of Tasmania, 1983.
 (40) Wiles, D. B.; Young, R. A. *J. Appl. Crystallogr.* **1981**, *14*, 149.
 (41) Saillant, R.; Jackson, R. B.; Streib, W. E.; Folting, K.; Wentworth, R. A. *D. Inorg. Chem.* **1971**, *10*, 1453.
 (42) Grey, I. E. Ph.D. Thesis, University of Tasmania, 1969.
 (43) Dubicki, L.; Krausz, E.; Stranger, R.; Smith, P. W.; Tanabe, Y. *Inorg. Chem.* **1987**, *26*, 2247.
 (44) Cotton, F. A.; Ucko, D. A. *Inorg. Chim. Acta* **1972**, *6*, 161.
 (45) Subbotina, M. Yu.; Aslanov, L. A. *Russ. J. Inorg. Chem. (Engl. Transl.)* **1985**, *30*, 816.
 (46) Gatehouse, B. M., Monash University. Private communication.
 (47) Furlani, C.; Piovesana, O. *Mol. Phys.* **1965**, *9*, 341.
 (48) Flint, C. D.; Paulusz, A. G. *Mol. Phys.* **1981**, *44*, 925.
 (49) Earnshaw, A. *Introduction to Magnetochemistry*; Academic Press: New York, 1968; p 77.
 (50) Harris, E. A. *J. Phys. C* **1972**, *5*, 338.
 (51) Gutowski, M. *Phys. Rev. B* **1977**, *18*, 5984.
 (52) Hay, P. J.; Thibeault, J. C.; Hoffmann, R. *J. Am. Chem. Soc.* **1975**, *97*, 4884.
 (53) Anderson, P. W. *Phys. Rev.* **1959**, *115*, 2.
 (54) Golding, R. M. *Applied Wave Mechanics*, D. Van Nostrand Co. Ltd.: London, 1969; p 166.
 (55) Richardson, J. W.; Blackman, M. J.; Ranochak, J. E. *J. Chem. Phys.* **1973**, *58*, 3010.
 (56) *International Tables for X-ray Crystallography*; Kynoch Press: Birmingham, England, 1974; Vol. IV.

- (57) Earnshaw, A. *Introduction to Magnetochemistry*, Academic Press: New York, 1968; pp 5, 6.
 (58) Hill, R. J.; Howard, C. J. *J. Appl. Crystallog.* **1985**, *18*, 173.

Table I. Structural Data for $(MeNH_3)_3Mo_2Cl_9$

formula	$C_3H_{18}N_3Mo_2Cl_9$
mol wt	607.15
cryst system	orthorhombic
space group	$Cmcm$ ($Z = 4$)
cell params, Å: $a; b; c$	7.1871 (3); 15.0864 (7); 17.6492 (8)
$V, \text{Å}^3$	1913.6
$d(\text{calc}), \text{g}\cdot\text{cm}^{-3}$	2.11
Mo 8(f): $y; z; B, \text{Å}^2$	0.1974 (2); 0.3258 (1); 2.06 (8)
Cl(1) 8(g): $x; y; B, \text{Å}^2$	0.2491 (9); 0.2679 (4); 2.8 (1)
Cl(2) 4(c): $y; B, \text{Å}^2$	0.0571 (6); 2.8 (1)
Cl(3) 16(h): $x; y; z; B, \text{Å}^2$	0.2331 (7); 0.1307 (3); 0.4009 (2); 2.9 (1)
Cl(4) 8(f): $y; z; B, \text{Å}^2$	0.3256 (4); 0.4068 (3); 2.9 (1)
N(1) 4(c): $y; B, \text{Å}^2$	0.563 (2); 2.4 (4)
N(2) 8(f): $y; z; B, \text{Å}^2$	0.823 (1); 0.060 (1); 2.4 (4)
C(1) 4(c): $y; B, \text{Å}^2$	0.483 (3); 6.3 (7)
C(2) 8(f): $y; z; B, \text{Å}^2$	0.914 (2); 0.092 (1); 6.3 (7)
$R_{\text{prof}}, \%$	5.46
$R_{\text{wt prof}}, \%$	7.25
$R_{\text{exp}}, \%$	1.89
$R_{\text{Bragg}}, \%$	4.21
data range (2θ), deg	16–90
no. of contributing reflens	444
no. of deg of freedom	1815

AX_3 having a six-layer stacking sequence $hcchc$. The M^{3+} ions occupy two-thirds of the octahedral sites between hexagonal (h) and cubic (c) stacked layers. The MX_6^{3-} octahedra share a common trigonal face across h layers and so form discrete $M_2X_9^{3-}$ binuclear anions. The packing arrangement of A and X atoms is shown in Figure 1.

We have recently described the effect of change in A cation size on the geometry of the $M_2X_9^{3-}$ anion.³⁵ Whereas increase in size of the A(2) cation is simply accommodated by displacement of the binuclear anions, increase in size of the A(1) cation, lying in the plane of the bridging halogens, results in an expansion of the binuclear unit along [0001] with accompanying increase in the M–M separation. The axial distortion of the binuclear anion resulting from a change in cation size can be measured by using the structural moduli d'/d'' , $(90 - \alpha)^\circ$, and $(\theta - 70.53)^\circ$ ⁴⁴ shown in Figure 2. The first parameter ratio measures the displacement of the M^{3+} ions from the centroids of their octahedra, where d' and d'' correspond to the M–h and M–c layer separations, respectively. The remaining two angular moduli measure the amount by which the X(1)–M–X(1) and M–X(1)–M bond angles deviate from their ideal values of $\alpha = 90^\circ$ and $\theta = 70.53^\circ$, respectively. In Figure 2, $(\theta - 70.53)^\circ$ is plotted against d'/d'' for all $A_3Mo_2X_9$ compounds examined in this study. The results for $Cs_3Cr_2X_9$ ($X = Cl, Br$)⁴¹ and $A_3W_2Cl_9$ ($A = Cs, K$)^{34,35} are also included for comparison. The majority of Mo compounds fall within the lower left quadrant, indicative of appreciable M–M interaction.

Structures Containing Nonsymmetric Cations. The results of a single-crystal structure refinement of $(EtNH_3)_3Mo_2Cl_9$ were recently communicated to us.⁴⁶ Using the coordinates of the Mo and Cl atoms in this structure as starting values, we refined the structure of the isostructural monomethylammonium salt using the Rietveld method. The results of the structure determination of $(MeNH_3)_3Mo_2Cl_9$ are given in Tables I and II, the latter detailing bond distances and angles relevant to the $Mo_2Cl_9^{3-}$ anion. Values are also given for the Cs salt⁴¹ to provide a measure of the distortion away from D_{3h} symmetry for the $MeNH_3$ salt. The observed, calculated, and difference diffraction profiles for the methylammonium salt are shown in Figure 3, while a plot of the structure viewed approximately along the [100] direction is shown in Figure 4.

The gross features of the X-ray powder patterns of both $(BuNH_3)_3Mo_2Cl_9$ and $(HexNH_3)_3Mo_2Cl_9$ initially indicated they were isostructural with the ethylammonium salt, but closer examination revealed reflections of type $0kl, k \neq 2n$, which violate

Table II. Interatomic Distances and Angles for $A_3Mo_2Cl_9$ ($A = Cs, MeNH_3$)

	$Cs_3Mo_2Cl_9^a$	$(MeNH_3)_3Mo_2Cl_9$
Distances (Å)		
Mo–Cl(1)	2.49 (1)	2.475 (6)
Mo–Cl(2)	2.49 (1)	2.504 (8)
Mo–Cl(3)	2.384 (6)	2.361 (5)
Mo–Cl(4)	2.384 (6)	2.405 (6)
Cl(1)–Cl(1)	3.643 (8)	3.61 (1)
C6(1)–Cl(2)	3.643 (8)	3.65 (1)
Cl(3)–Cl(3)	3.401 (6)	3.35 (1)
Cl(3)–Cl(4)	3.401 (6)	3.386 (7)
Mo–Mo	2.66 (1)	2.675 (4)
Angles (deg)		
Mo–Cl(1)–Mo	64.5 (3)	65.4 (2)
Mo–Cl(2)–Mo	64.5 (3)	64.6 (2)
Cl(1)–Mo–Cl(1)	94.2 (1)	92.7 (2)
Cl(1)–Mo–Cl(2)	94.2 (1)	94.3 (1)
Cl(3)–Mo–Cl(3)	91.0 (3)	90.4 (2)
Cl(3)–Mo–Cl(4)	91.0 (3)	90.5 (1)
Cl(1)–Mo–Cl(4)	87.4 (2)	88.6 (2)
Cl(2)–Mo–Cl(3)	87.4 (2)	86.5 (1)

^aData taken from ref 41.

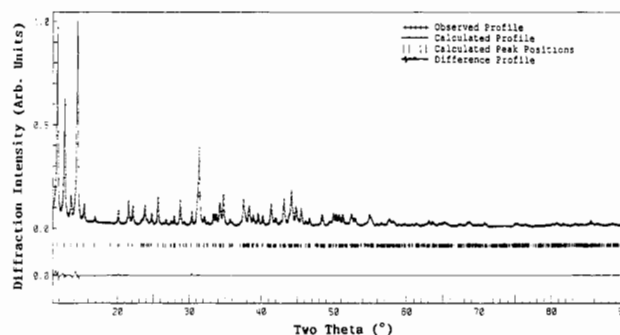


Figure 3. Rietveld profile plot for $(MeNH_3)_3Mo_2Cl_9$. Crosses correspond to the observed intensity, the solid line corresponds to the calculated profile fit, and tick marks correspond to the calculated peak positions. The bottom solid line is the difference profile corresponding to $I_{\text{obs}} - I_{\text{calc}}$.

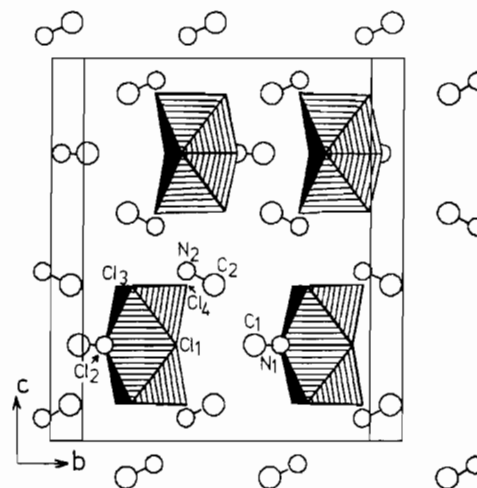


Figure 4. Structure of $(MeNH_3)_3Mo_2Cl_9$ viewed approximately down the [100] direction of the orthorhombic unit cell. The structure is rotated 10° from [100] around the c axis to show more clearly the polyhedral units. Cation A(1), shown as N_1C_1 , is seen to pack in the plane of the bridging halogens.

the extinction conditions for $Cmcm$. However, these reflections were very weak, indicating that the departure from $Cmcm$ is quite small. Rietveld refinements were not undertaken due to the likely disorder of the alkylammonium groups, but the unit cell dimensions were determined from the X-ray powder patterns and are given in Table III along with the values for the NH_4 , $MeNH_3$, and $EtNH_3$ salts. The b axis values calculated on the assumption of

Table III. Unit Cell Dimensions for (RNH₃)₃Mo₂Cl₉ (R = H, Me, Et, Bu, Hex)

complex salt	a, Å	b, Å	c, Å	b _{hex} , Å ^a
(NH ₄) ₃ Mo ₂ Cl ₉	7.135	12.358	16.993	12.358
(MeNH ₃) ₃ Mo ₂ Cl ₉	7.185	15.081	17.645	12.445
(EtNH ₃) ₃ Mo ₂ Cl ₉ ^b	7.226	17.720	17.916	12.516
(BuNH ₃) ₃ Mo ₂ Cl ₉	7.298	21.220	18.203	12.641
(HexNH ₃) ₃ Mo ₂ Cl ₉	7.372	25.670	18.358	12.769

^a Calculated by assuming an orthohexagonal cell where b_{hex} = √3a_{ortho}. ^b Private communication.⁴⁶

an exact hexagonal cell, where b_{hex} = √3a_{ortho}, are also given for comparison.

Magnetic Studies. The temperature dependence of magnetic susceptibility between 90 and 350 K was measured for the complex salts A₃Mo₂Cl₉ (A = Rb, NH₄, MeNH₃, Me₂NH₂, Me₃NH, EtNH₃, Et₂NH₂, Et₄N, BuNH₃, HexNH₃), (Me₄N)₃Mo₂Br₉, and A₃Mo₂I₉ (A = Cs, EtNH₃). In addition, susceptibility data is available on the complex salts A₃Mo₂Cl₉ (A = K, Cs, Et₃NH, PyH, PipeH)^{38,42} and A₃Mo₂Br₉ (A = Cs, Et₄N).⁴² The temperature dependence of magnetic susceptibility below 450 K can be fitted by using either the d²d² or d³d³ binuclear susceptibility equations⁴⁹ with identical results, as the S = 3 spin level is not significantly populated. However, in view of the large M–M σ bonding for this system,⁴³ the d²d² susceptibility equation

$$\chi_a = \frac{3K}{T} \left[\frac{5 + x^4}{5 + 3x^4 + x^6} \right] + N\alpha$$

is more appropriate, where $\chi_a = \chi_M/2$, $K = Ng^2\beta^2/3k$, $x = \exp(J_{ab}/kT)$, and $N\alpha$ is the temperature-independent paramagnetism (TIP) term. In most cases the g value was not refined but determined from room-temperature ESR measurements on powdered samples. The best fit values of J_{ab} , $N(\alpha)$, and g are detailed in Table IV along with the Mo–Mo distances when known.

Discussion

Structural Studies. The Rietveld refinement results³⁵ for A₃Mo₂X₉ complex salts containing spherical or pseudospherical univalent A cations clearly show the dependence of the Mo₂X₉³⁻ geometry on the size of the A cation, as is apparent from Table IV. From the packing arrangement within the unit cell, one predicts that an increase in A cation size only along the c axis direction of the unit cell will result in expansion of the binuclear anion. It is possible to test this prediction on the results obtained for the structurally related alkylammonium salts (RNH₃)₃Mo₂Cl₉ (R = Me, Et, Bu, Hex). These salts have been shown to crystallize in *Cmcm*, which is a subgroup of *P6₃/mmc* in which the majority of symmetric cation salts crystallize. As such, the packing of A, M, and X in the monoalkylammonium salts resembles the close-packing arrangement in *P6₃/mmc* structures. The *Cmcm* structure differs from *P6₃/mmc* in that the triangular grouping of halogens in both terminal and bridging sites are no longer symmetry related. The close-packing arrangement is distorted along the b axis direction so that two inequivalent bridging and terminal halogen sites X(1), X(2) and X(3), X(4), respectively, are present. This distortion results in loss of trigonal symmetry of the binuclear anion and leads to gaps in the close-packing arrangement along [0k0]. The size of these gaps is given by the deviation of the b axis length from the ortho-hexagonal dimension of √3a. Analogous to the hexagonal structures, two distinct cation sites A(1) and A(2) are present, as can be seen from Figure 4, with cation A(1) packing in the plane of the bridging halogens. The distortion of the binuclear anion in the MeNH₃ salt from D_{3h} to C_{2v} site symmetry is shown by a comparison of bond lengths and angles with those for the Cs salt (D_{3h} site symmetry) given in Table II. Overall, the C_{2v} distortion is relatively small with the majority of interatomic distances and angles close in value to those for Cs₃Mo₂Cl₉.

The crystal structures of the MeNH₃ and EtNH₃ salts, as well as a comparison of the unit cell dimensions given in Table III, clearly show that the alkyl group in the monoalkylammonium salts

Table IV. Magnetic Parameters for A₃Mo₂X₉ Salts

complex salt	Mo–Mo, Å	-J _{ab} , cm ⁻¹	10 ⁶ Nα, cm ⁻¹	g value	ref
Symmetric Cation Salts					
K ₃ Mo ₂ Cl ₉	2.524	560	79	2.01	35, 42
Rb ₃ Mo ₂ Cl ₉	2.590	491	24	1.98 ^a	35
(NH ₄) ₃ Mo ₂ Cl ₉	2.600	471	12	1.95	35
Cs ₃ Mo ₂ Cl ₉	2.655	414	44	1.96	35, 41, 42
(Me ₄ N) ₃ Mo ₂ Cl ₉	2.778	275	210	1.95	35
(Et ₄ N) ₃ Mo ₂ Cl ₉		237	38	1.96	42
K ₃ Mo ₂ Br ₉	2.57				35
Rb ₃ Mo ₂ Br ₉	2.731				35
Cs ₃ Mo ₂ Br ₉	2.816	380	147	1.99	35, 41, 42
(Me ₄ N) ₃ Mo ₂ Br ₉	3.106	239	252	2.05 ^a	35
(Et ₄ N) ₃ Mo ₂ Br ₉		215	232	2.06	42
Cs ₃ Mo ₂ I ₉	3.070	467	442	1.97	35, 39
Asymmetric Cation Salts					
(MeNH ₃) ₃ Mo ₂ Cl ₉	2.665	410	69	1.95	
(EtNH ₃) ₃ Mo ₂ Cl ₉	2.670	393	86	1.95	46
(BuNH ₃) ₃ Mo ₂ Cl ₉		388	54	1.95	
(HexNH ₃) ₃ Mo ₂ Cl ₉		343	57	1.95	
(Me ₂ NH ₂) ₃ Mo ₂ Cl ₉		323	137	1.95	
(Et ₂ NH ₂) ₃ Mo ₂ Cl ₉		310	113	1.95	
(Me ₃ NH) ₃ Mo ₂ Cl ₉		289	81	2.09 ^a	
(Et ₃ NH) ₃ Mo ₂ Cl ₉		279	34	1.95	42
(PipeH) ₃ Mo ₂ Cl ₉	2.734	267	64	1.95	38, 45
(PyH) ₃ Mo ₂ Cl ₉	2.685	341			38, 45
(EtNH ₃) ₃ Mo ₂ I ₉		477	557	1.98	39

^a g value refined in susceptibility fit.

orientates along the b axis of the orthorhombic unit cell. Examination of Table IV shows that the increase in cation size from MeNH₃ to EtNH₃ has had negligible effect on the Mo–Mo separation. This observation is in agreement with the earlier prediction that only a size increase of the A(1) cation in the direction of the c axis would result in expansion of the binuclear unit.

Metal–Metal Bonding. Previous magnetic studies^{36–39} on A₃Mo₂X₉ complexes have assumed that all three d electrons on each Mo center are active in the exchange-coupling process and therefore have ignored the possibility of strong M–M σ bonding. The detailed analysis of the electronic spectrum of Cs₃Mo₂Cl₉⁴³ has shown that the excited-state spectrum below 16 000 cm⁻¹ can be attributed to pair states derived from an effective t_{2e}²t_{2c}² configuration where the t_{2z} orbitals on each Mo center are involved in a M–M σ bond. However, although the σ interaction is strong, the t_{2z} electrons are not fully paired off, and as a result, the ground-state exchange is still dominated by the σ contribution. This is in contrast to the fully paired case where only the M–M π interaction can contribute to the ground exchange coupling. In order to appreciate the role of significant M–M interaction in Mo₂X₉³⁻ complexes, the effects of the single-ion and pair-interaction parameters on the ground-state exchange splitting are now examined. Details of the method of calculation have already been given.⁴³

For a weakly coupled pair system where the single-ion ground state is orbitally nondegenerate, the pair levels can in most cases be adequately described by the well known HDVV spin Hamiltonian

$$H_{ex} = -2J_{ab}S_a \cdot S_b \quad (1)$$

where J_{ab} is the exchange integral defined by

$$J_{ab} = \sum_{ij} J_{ij}/4S_a S_b \quad (2)$$

and the energies of the pair spin levels are given by

$$E(S) = J_{ab}S(S + 1) \quad (3)$$

In (2) J_{ab} takes the average value summed over all possible exchange pathways, which are parametrized by the orbital-dependent exchange parameters J_{ij} . To second order one obtains

$$J_{ij} = \langle \phi_i(1) \phi_j(2) | e^2/r_{12} | \phi_i(2) \phi_j(1) \rangle - 2h(i,j)^2/U \quad (4)$$

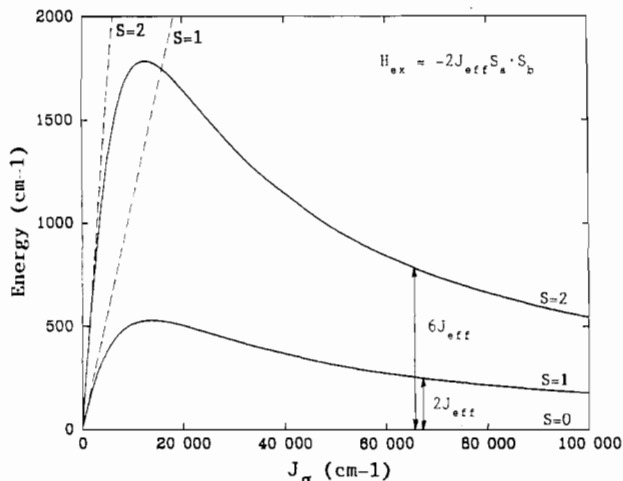


Figure 5. The energy of $t_2^3t_2^3$ ground-state pair spin levels as a function of J_σ . The energies of $S = 1, 2$ spin levels are plotted relative to that of the $S = 0$ spin state. Dashed lines correspond to the energies of $S = 1, 2$ pair spin states calculated from HDVV model (3). Single-ion parameters are set at $B = 467 \text{ cm}^{-1}$, $C = 4B$, $Dq = 1920 \text{ cm}^{-1}$, $K = 0$, $\zeta = 0$, and $J_x = 0$. For large J_σ the pair spin levels still approximately obey a Landé type interval separation in terms of J_{eff} .

The first term on the right corresponds to potential exchange and is purely electrostatic in nature. The second term corresponds to kinetic exchange and involves the transfer integral $h(i,j)$ as well as the energy denominator U , which gives the average Coulombic repulsion between the two electrons when located on the same metal ion.

Configuration interaction results in a deviation of the pair spin levels from a Landé interval separation given by (3). In the case of moderate to strong M-M-bonding interactions, the off-diagonal exchange coupling can lead to extensive configuration interaction between different multiplets. In this case the validity of a simple HDVV description of the ground-pair levels is questionable. To examine this situation, the energies of the ground-state spin levels were calculated by using the full $t_2^3t_2^3$ pair basis. Their dependence on J_σ ($= -2J_{zz}$) is shown in Figure 5. For this set of calculations the single-ion parameters were given the values $B = 467 \text{ cm}^{-1}$, $C = 4B$, $Dq = 1920 \text{ cm}^{-1}$, $K = 0$, and $\zeta = 0$. The values of the Racah and cubic field parameters are those appropriate to the electronic spectrum of cubic $MoCl_6^{3-}$ moieties.^{47,48} The spin-orbit coupling and trigonal-field parameters were arbitrarily set to zero, since for large J_σ their effect on the ground spin levels is negligible.

As J_σ increases, there is a corresponding increase in the energies of the ground-state $S = 1, 2, 3$ spin levels relative to the $S = 0$ spin state. However, the energies of the $S = 1, 2$ spin levels reach a maximum around $J_\sigma = 15000 \text{ cm}^{-1}$ and then gradually fall off to zero as $J_\sigma \rightarrow \infty$. The dashed lines in Figure 5 correspond to the spin-state energies (eq 3) calculated on the basis of the simple HDVV Hamiltonian (eq 1). Clearly, for $J_\sigma > 2000 \text{ cm}^{-1}$ the pair spin-state energies no longer obey (3) and the HDVV description of the ground-state spin levels is no longer adequate. In this case the magnitude of J_{ab} cannot be used as an indicator of weak or strong M-M interaction. For example, from Figure 5 the singlet-triplet separation for $J_\sigma \approx 63000 \text{ cm}^{-1}$ ($J_{zz} = -31500 \text{ cm}^{-1}$) results in $-J_{ab} = 125 \text{ cm}^{-1}$. However, from the HDVV model (eq 2) we have $J_{ab} = J_{zz}/9 = 3500 \text{ cm}^{-1}$, which is approximately 30 times larger. Clearly, when the M-M interaction is no longer weak, J_{ab} cannot be regarded as the average sum of all possible exchange pathways as given in (2).

The breakdown of the HDVV description of the ground spin levels results from the fact that for large J_σ the single-ion spins S_a and S_b are no longer good quantum numbers. This can be intuitively seen in the case where the σ exchange becomes so large that two electrons, one on each metal center, are fully paired off in a M-M σ bond. In this case the exchange coupling within the ground-state spin manifold will be described by the HDVV Hamiltonian (eq 1) but with $S_a = S_b = 1$, not $3/2$. However, one can envisage the intermediate situation where the σ exchange is

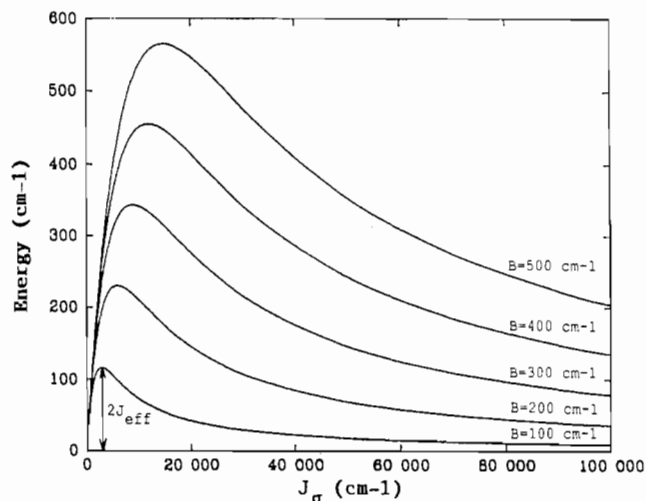


Figure 6. Dependence of ground-state exchange on the Racah B single-ion electron repulsion parameter. The energy of $S = 1$ pair spin state is shown relative to that of the $S = 0$ spin level. Calculations are for $C = 4B$, $Dq = 1920 \text{ cm}^{-1}$, $K = 0$, $\zeta = 0$, and $J_x = 0$.

not large enough to fully pair off electrons into a M-M σ bond. In this realm the single-ion spins take on effective values ranging from $S_a = S_b = 3/2$ through $S_a = S_b = 1$ in the σ -bonded case. Although the HDVV description of the ground spin levels breaks down as J_σ increases, the remaining $S = 0, 1, 2$ pair spin levels continue to obey an approximate Landé type interval separation given by

$$E(S) = -2J_{\text{eff}}S(S+1) \quad (5)$$

where J_{eff} is an effective exchange integral that does not conform to (2).

For weakly coupled pair systems the exchange splitting of the ground-pair levels is only dependent on the magnitudes of the various orbital-exchange parameters J_{ij} . However, as J_σ increases, the ground-state exchange splitting becomes increasingly sensitive to the single-ion electron repulsion parameters. To illustrate this, the effect of the single-ion Racah B electron repulsion parameter on the energy of the $S = 1$ ground spin level is shown in Figure 6. As B is lowered from 500 to 100 cm^{-1} , the energy of the $S = 1$ spin state is markedly reduced for any constant value of J_σ . Although not shown, the same trend is also observed for the $S = 2$ pair spin state. Of course, near either extreme limit where $J_\sigma \rightarrow 0$ or $J_\sigma \rightarrow \infty$, the exchange splitting becomes independent of these parameters.

The Racah parameters are related to the single-ion Coulomb and exchange integrals $C(i,j)$ and $K(i,j)$, respectively. Using the transformations

$$\begin{aligned} t_{2x} &= \frac{\sqrt{2}}{\sqrt{3}}(x^2 - y^2) - \frac{1}{\sqrt{3}}(xz) \\ t_{2y} &= \frac{-\sqrt{2}}{\sqrt{3}}(xy) - \frac{1}{\sqrt{3}}(yz) \\ t_{2z} &= z^2 \end{aligned} \quad (6)$$

where t_{2x} , t_{2y} , and t_{2z} are the real trigonal t_2 orbitals expressed in terms of cubic t_2 orbitals quantized down the C_3 axis, we can express the trigonal electrostatic integrals in terms of the Racah parameters as

$$\begin{aligned} C(x,x) &= C(y,y) = C(z,z) = A + 4B + 3C \\ C(x,y) &= C(x,z) = C(y,z) = A - 2B + C \\ K(x,y) &= K(x,z) = K(y,z) = 3B + C \end{aligned} \quad (7)$$

Anisotropy in electron repulsion will result in a further distinction

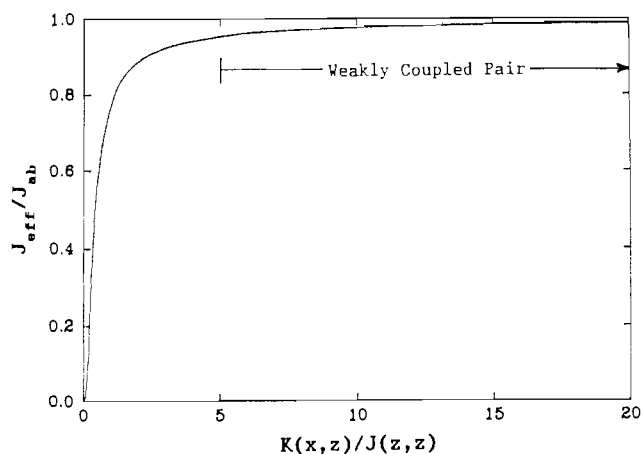


Figure 7. Effect of single-ion Coulombic exchange $K(x,z)$ on the pair ground-state exchange. The parameter ratio $K(x,z)/J(z,z)$ is a measure of the single-ion Coulombic exchange relative to the pair-exchange parameter $J(z,z) = -J_\sigma/2$. Weakly coupled pair applies when $J_{\text{eff}} = J_{\text{ab}}$ and $K(x,z)/J(z,z) > 5$. A similar plot also occurs for $K(x,z)/J(x,x)$ where $J(x,x) = -J_\pi/18$.

between electrostatic integrals involving the trigonal t_{2z} orbital and those which do not.

The ground-state exchange splitting is found to be dependent on the single-ion exchange integrals $K(x,z) = K(y,z)$ as shown in Figure 7, where the parameter ratio $J_{\text{eff}}/J_{\text{ab}}$ is plotted against $K(x,z)/J(z,z)$. A similar plot also occurs for $K(x,z)/J(x,x)$. The latter two parameter ratios are simply a measure of the single-ion Coulombic exchange relative to the pair-exchange parameters $J(z,z) = -J_\sigma/2$ and $J(x,x) = -J_\pi/18$.⁴³ The former ratio $J_{\text{eff}}/J_{\text{ab}}$ is a measure of the deviation away from a weakly coupled pair for which $J_{\text{eff}} = J_{\text{ab}}$. It is apparent that as J_σ is increased, J_{eff} is progressively reduced in value relative to J_{ab} . Deviation from the weakly coupled pair approximation is observed to occur when either $K(x,z)/J(z,z)$ or $K(x,z)/J(x,x)$ is less than 5. In general, the weakly coupled pair approximation should apply when the single-ion exchange is approximately 5 times greater than the largest pair-exchange integral.

Magnetic Susceptibility. Consideration of M–M bonding effects in $A_3Mo_2X_9$ complex salts implies that the d^3d^3 binuclear susceptibility equation⁴⁹ may not be appropriate in the analysis of the magnetic susceptibility. In fact, depending on the extent of M–M interaction, the effective exchange can vary anywhere between a d^0d^0 and d^3d^3 spin-coupled system. From (7) the single-ion exchange integral is given by $K(x,z) = 3B + C \approx 7B$. Since for $MoCl_6^{3-}$ moieties B is approximately 470 cm^{-1} , we have $K(x,z) \approx 3300 \text{ cm}^{-1}$. For $Cs_3Mo_2Cl_9$ a value of $J_{\text{ab}} = -420 \text{ cm}^{-1}$ was obtained.³⁷ Assuming that the ground-state exchange is dominated by the M–M σ interaction, we have $J_{\text{ab}} \approx J(z,z)/9 = -420 \text{ cm}^{-1}$, and therefore $J(z,z) \approx 3800 \text{ cm}^{-1}$. From these experimental values one obtains the ratio $K(x,z)/J(z,z) = 0.87$, indicating significant departure from a weakly coupled $t_2^3t_2^3$ pair. Furthermore, from the analysis of the electronic spectrum J_σ is approximately $20000 \pm 5000 \text{ cm}^{-1}$. Using the HDVV model (eq 2), one obtains $-J_{\text{ab}} = J_\sigma/18 \approx 2200 \text{ cm}^{-1}$. Since this value is over 5 times greater than the observed value, it is clear that the HDVV model does not apply.

In order to determine which $d^n d^n$ -coupled model is appropriate to describe the ground exchange coupling in $A_3Mo_2X_9$ complexes, it is first necessary to appreciate how the theoretical susceptibility curves will differ in each case. To show these differences, the temperature dependence of magnetic susceptibility is shown in Figure 8 for d^1d^1 , d^2d^2 , and d^3d^3 spin-coupled systems with $-J_{\text{ab}} = 200$ and 400 cm^{-1} . In these calculations the g value was set at the spin only value of 2.0 while the temperature-independent term $N\alpha$ was arbitrarily set to zero. For $-J_{\text{ab}} = 200 \text{ cm}^{-1}$ the d^1d^1 susceptibility curve begins to separate from the d^2d^2 and d^3d^3 curves at around 250 K whereas for $-J_{\text{ab}} = 400 \text{ cm}^{-1}$ this does not occur until approximately 450 K. Much higher temperatures are required to distinguish between the d^2d^2 and d^3d^3 susceptibility

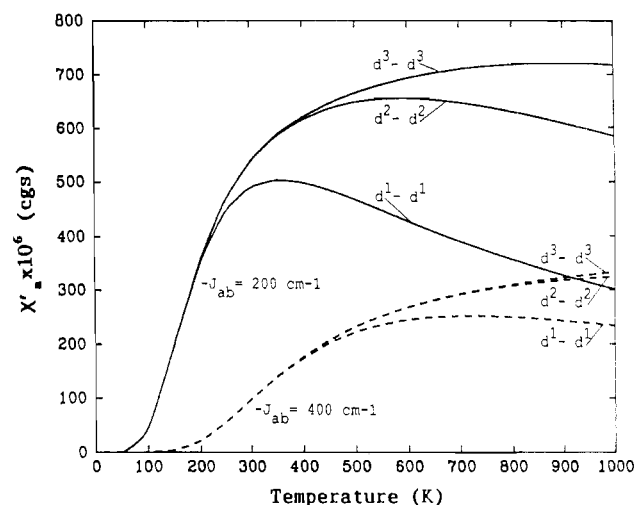


Figure 8. Theoretical temperature dependence of magnetic susceptibility for $d^n d^n$ ($n = 1-3$) spin-coupled models. The solid lines are for $-J_{\text{ab}} = 200 \text{ cm}^{-1}$, and the dashed lines, for $-J_{\text{ab}} = 400 \text{ cm}^{-1}$. For all curves $N\alpha = 0$ and $g = 2$.

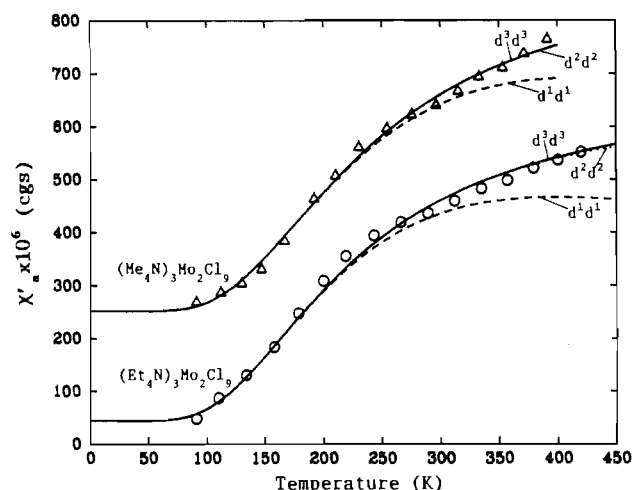


Figure 9. Temperature dependence of magnetic susceptibility for $(Et_4N)_3Mo_2Cl_9$ and $(Me_4N)_3Mo_2Br_9$. Theoretical curves shown correspond to the best fits for d^1d^1 (dashed), d^2d^2 (dotted), and d^3d^3 (solid) spin-coupled models. Above 250 K the d^1d^1 model no longer gives a satisfactory fit to experimental data.

curves. For $-J_{\text{ab}} = 200 \text{ cm}^{-1}$ this separation occurs around 450 K whereas for $-J_{\text{ab}} = 400 \text{ cm}^{-1}$ no separation is apparent below 800 K.

From Figure 8 it is obvious that susceptibility measurements on $A_3Mo_2X_9$ complexes need to be taken up to relatively high temperatures in order to determine which $d^n d^n$ spin-coupled model is applicable. Unfortunately, for both the alkali-metal and alkylammonium salts of $Mo_2X_9^{3-}$, the temperatures required to discriminate between the d^2d^2 and d^3d^3 models are in excess of their respective melting or decomposition points. However, for both the chloride and bromide complexes, it is possible to show that the d^1d^1 spin-coupled model does not apply. In order to demonstrate this, the magnetic susceptibility of $(Et_4N)_3Mo_2Cl_9$ and $(Me_4N)_3Mo_2Br_9$ were measured up to 450 K and are shown in Figure 9. The best fit susceptibility curves calculated for d^1d^1 , d^2d^2 , and d^3d^3 spin-coupled models are also plotted. It is clear that at temperatures above 250 K the d^1d^1 model no longer provides a satisfactory fit to the observed magnetic susceptibility. The difference between the d^2d^2 and d^3d^3 models on the other hand is virtually imperceptible, indicating that the $S = 3$ level, if present, is not significantly populated. As such, the magnetic susceptibility data fit to the d^3d^3 model cannot be used as evidence for the absence of a M–M σ bond.

Magneto-Structural Correlations. The structural results for the alkali-metal and tetraalkylammonium salts of $Mo_2Cl_9^{3-}$ clearly

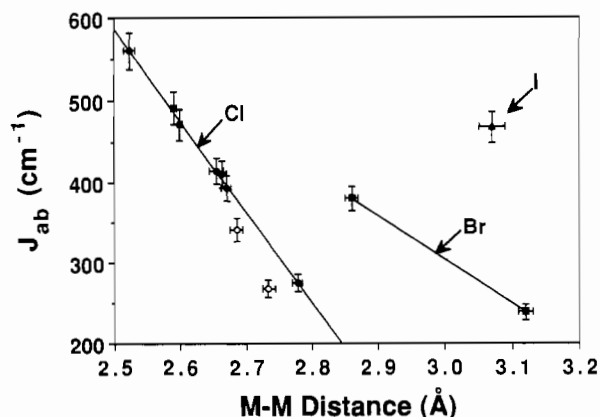


Figure 10. Correlation between ground-state exchange constant J_{ab} and metal-metal separation in $A_3Mo_2X_9$ complexes. Open circles are points plotted for the pyridinium and piperidinium salts of $Mo_2Cl_9^{3-}$.^{38,45}

show a progressive increase in the Mo-Mo separation as the size of the univalent A cation increases. This in turn leads to a reduction in the magnetic exchange, as is confirmed by the data given in Table IV. In fact, if we range from the K salt through to the Et_4N salt of $Mo_2Cl_9^{3-}$, the value of $-J_{ab}$ has decreased by a factor of 3, corresponding to an observed increase in the Mo-Mo separation of over 0.25 Å. The dependence of J_{ab} on the M-M separation is shown in Figure 10 and is approximately linear for the chloride complexes examined in this study. The linear dependence of J_{ab} on the Mo-Mo separation is unlikely to continue as J_{ab} approaches zero, since for large M-M distances superexchange processes involving bridging ligands will compete favorably with direct exchange pathways as a result of negligible M-M orbital overlap. Even so, the observed linear dependence between J_{ab} and Mo-Mo separation is not without precedence, since similar trends have been observed for Mn^{2+} - and Cr^{3+} -doped metal oxides.^{50,51}

Although the complex salts containing nonsymmetric A cations no longer adopt hexagonal structures, examination of Table IV shows that there is still a decrease in $-J_{ab}$ with increasing size of the A cation, although the trend is not as dramatic as first might be expected on consideration of the relative sizes of these cations. For instance, $-J_{ab}$ decreases by only 20 cm^{-1} in going from the $MeNH_3$ to $BuNH_3$ salt. However, these magnetic results are consistent with the structural findings in that the alkyl group is directed along the b axis of the orthorhombic unit cell, leading to similar M-M distances and magnetic exchange in these salts.

As seen from Figure 10, the pyridinium and piperidinium salts of $Mo_2Cl_9^{3-}$ ^{38,45} deviate slightly from the linear correlation observed for all other chloro salts examined in this study. However, both these salts bear little resemblance to the close-packing arrangement in the hexagonal structures. Furthermore, the $Mo_2Cl_9^{3-}$ anion is considerably distorted from trigonal symmetry and as a result the M-M π interaction will be asymmetric ($J_{xx} \neq J_{yy}$).

The extent of magnetic exchange in $A_3Mo_2X_9$ salts is clearly sensitive to the halogen type X. From Figure 10 the observed magnetic exchange increases in the order $Cl < Br < I$ for any given M-M separation. This is not unexpected as the single-ion electron repulsion is reduced in going from the Cl to I complexes; consequently, the metal ion d orbitals are dilated, leading to increased M-M orbital overlap and antiferromagnetic exchange. In addition, superexchange pathways will be more efficient due to the increased metal-ligand orbital overlap.

Modeling the Correlation. Since the M-M interaction in $Mo_2X_9^{3-}$ complexes is significant, it is instructive to approach the problem from a molecular orbital perspective. For a binuclear system involving pairwise molecular orbital interactions with one electron in each of the two single-ion orbitals involved, the spin singlet-triplet separation Δ_{10} is given by⁵²

$$\Delta_{10} = -2J_{ab} = -2K_{ab} + \frac{(\epsilon - \epsilon^*)^2}{C_{aa} - C_{ab}} \quad (8)$$

where K_{ab} is the two-center Coulombic exchange integral defined by

$$K_{ab} = \langle \phi_a(1) \phi_b(2) | 1/r_{12} | \phi_b(1) \phi_a(2) \rangle$$

C_{aa} and C_{ab} are the one- and two-center Coulomb integrals, respectively, defined by

$$C_{aa} = \langle \phi_a(1) \phi_a(2) | 1/r_{12} | \phi_a(1) \phi_a(2) \rangle$$

$$C_{ab} = \langle \phi_a(1) \phi_b(2) | 1/r_{12} | \phi_a(1) \phi_b(2) \rangle$$

and ϵ and ϵ^* are the bonding and antibonding MO energies, respectively. In the above expression ϕ_a and ϕ_b refer to orthogonalized MO's localized on centers a and b, respectively.

According to Anderson's treatment of superexchange,⁵³ Δ_{10} is given by

$$\Delta_{10} = -2J_{ab} = -K_{ab} + \frac{4h(a,b)^2}{C_{aa} - C_{ab}} \quad (9)$$

where $h(a,b)$ is the transfer integral common to kinetic exchange and the denominator $C_{aa} - C_{ab}$ corresponds to U in expression 4. Equating expressions 8 and 9, one obtains

$$2h(a,b) = \epsilon - \epsilon^* \quad (10)$$

implying the equivalence of Anderson's transfer integral to the pair-wise bonding-antibonding MO separation. Substituting (10) into (2) and neglecting potential exchange terms, one obtains

$$J_{ab} = -1/9[(\epsilon_z - \epsilon_z^*)^2/2U_z + (\epsilon_x - \epsilon_x^*)^2/U_x] \quad (11)$$

Ignoring configuration interaction, one obtains the bonding and antibonding energies for each MO pair by solving the appropriate two by two secular equation involving metal centers a and b. For the symmetrical case, one obtains the result

$$\epsilon^* - \epsilon = \frac{2(H_{ab} - H_{aa}S)}{1 - S^2} \quad (12)$$

where the H_{ij} are matrix elements involving the single-ion and pair kinetic and potential energy terms and S is the overlap integral. For relatively small overlaps ($S^2 \ll 1$) the approximation $1 - S^2 = 1$ is valid. Furthermore, the transfer or resonance integral H_{ab} is usually approximated⁵⁴ by

$$H_{ab} = F(H_{aa} + H_{bb})S/2 \quad (13)$$

where F is a constant. On the incorporation of the above approximations, expression 12 reduces to

$$\epsilon - \epsilon^* = 2H_{aa}(1 - F)S \quad (14)$$

implying that the bonding-antibonding MO separation is proportional to the overlap integral S . In order to relate J_{ab} to the various MO overlaps, expression 14 is simply substituted into (11), giving the result

$$J_{ab} = -1/9[a_1S_z^2/2 + a_2S_x^2] \quad (15)$$

where

$$a_i = 4H_{ii}^2(1 - F)^2/U_i$$

From the transformations given in (6), the trigonal t_{2g} M-M orbital overlaps are given by

$$S_z = \langle z^2 | z^2 \rangle = S_\sigma$$

$$S_x = S_y = 2/3(x^2 - y^2|x^2 - y^2) + 1/3(xz|xz) = 2/3S_\delta + 1/3S_\pi \quad (16)$$

Substituting the above relations into (15) gives the desired result

$$-J_{ab} = 1/9[a_1S_\sigma^2/2 + a_2(S_\pi^2 + 4S_\delta^2 + 2S_\pi S_\delta)/9] \quad (17)$$

where J_{ab} is expressed in terms of the cubic M-M orbital overlaps

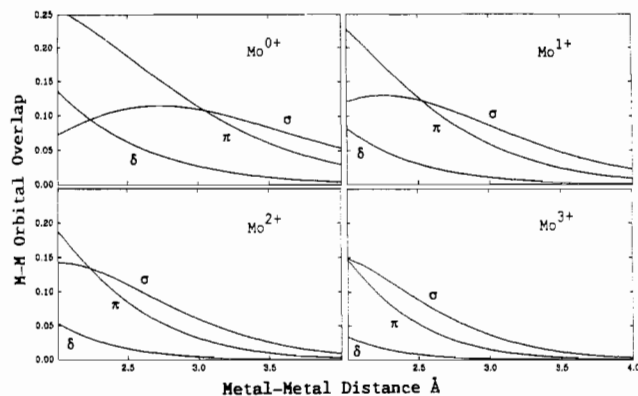


Figure 11. Metal-metal σ , π , and δ orbital overlaps for Mo^{n+} ($n = 0-3$).

Table V. Best Fit a_i Coefficients for Cl and Br Complexes

coeff	Mo^0	Mo^+	Mo^{2+}	Mo^{3+}
		Chloride		
a_0	a	-518	-78	78
a_1	a	3934	3077	3791
		Bromide		
a_0	-568	27	127	171
a_1	4082	1867	2379	4261

^a Values for Mo^0 for the Cl series are not given due to poor fit.

quantized down the trigonal C_2^3 axis.

Using the SCF-AO's given by Richardson et al.,⁵⁵ one can calculate the σ , π , and δ M-M orbital overlaps for Mo^{n+} ($n = 0-3$) for internuclear separations between 2 and 4 Å. The results are plotted in Figure 11. From the calculated overlaps, expression 17 can be used to model the observed correlation in Figure 10. However, from (16) the trigonal π overlaps ($S_x = S_y$) are reduced to one-third and two-thirds of the cubic π and δ overlaps, respectively. In this respect, and in view of the much larger σ overlap in the 2.5-3.2-Å region, the M-M π and δ overlaps can be neglected. Accordingly, expression 17 reduces to

$$-J_{ab} = a_0 + a_1 S_\sigma^2 / 18 \quad (18)$$

where the term a_0 has been added to account for relatively constant superexchange contributions at large M-M distances.

The results listed in Table IV were fitted by using expression 18 with the formal charge on the Mo varying from zero to 3+ in integral steps. The best fit values of a_0 and a_1 for the chloride and bromide complexes are given in Table V. For the chloride complexes the best fit occurs for Mo^{1+} but the value of a_0 , apart from being negative, is too large considering its source should be predominantly from superexchange processes effective at large internuclear distances. In this respect, the values for Mo^{2+} and Mo^{3+} are more realistic. In fact, assuming $a_0 \approx 0$ for the chloride series, the charge on the Mo will be approximately 2.5+ and this seems quite reasonable.

For comparison the best fits are shown in Figure 12 for all three halogen series with the charge on the Mo maintained at 3+. Since there was only one data point for the iodide series, no unique fit was possible. The increasing value of a_0 in the order $\text{Cl} < \text{Br} < \text{I}$ is expected, since the effective charge on the Mo should be lower for the bromide and iodide salts due to increased covalency effects

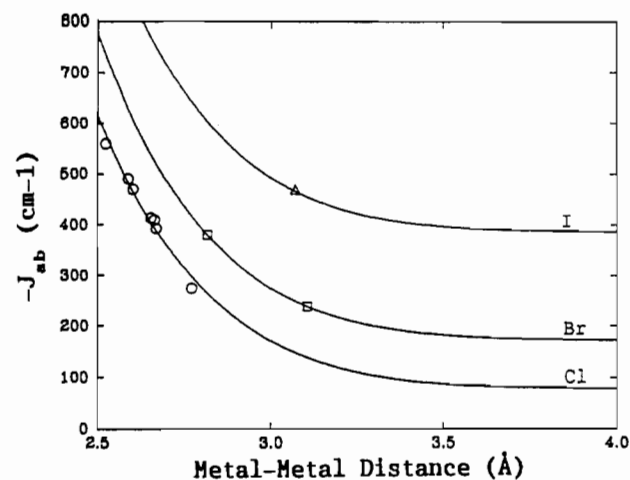


Figure 12. Metal-metal σ overlap fit to J_{ab} versus metal-metal separation correlation. Solid curves shown are calculated by using expression 18 on the basis of M-M σ overlaps for Mo^{3+} .

and therefore superexchange processes should be enhanced. The linear correlation between J_{ab} and M-M for the chloride series is simply a consequence of the narrow range of Mo-Mo distances involved. Increasing the internuclear separation beyond 2.8 Å should see a significant deviation from linearity for this series.

Conclusion

The variation in magnetic and structural properties exhibited in close-packed $\text{A}_3\text{Mo}_2\text{X}_9$ structures results from the unique packing effect of the A(1) cation in the plane of the bridging halogens. Increase in size of this cation along the c axis direction of the unit cell results in an expansion of the $\text{Mo}_2\text{X}_9^{3-}$ binuclear unit and consequently a reduction in the antiferromagnetic exchange coupling. Theoretical calculations have shown that a Heisenberg (HDVV) model of exchange coupling does not apply, even though the ground $S = 0, 1, 2$ pair spin levels still obey an approximate Landé separation. The observed correlation between J_{ab} and the M-M separation has been modeled by using a semi-quantitative molecular orbital approach based on the M-M σ orbital overlap.

Acknowledgment. We thank Dr. Bryan Gatehouse of Monash University, Melbourne, Australia, for communicating to us the results of the structure determination on $(\text{EtNH}_3)_3\text{Mo}_2\text{Cl}_9$. We also thank Ian Madsen of the Mineral Products Division, CSIRO, Melbourne, Australia, for help in relation to computing matters involving the Rietveld refinement of $(\text{MeNH}_3)_3\text{Mo}_2\text{Cl}_9$. Finally, R.S. gratefully acknowledges receipt of a Commonwealth of Australia postgraduate research award.

Registry No. $(\text{NH}_4)_3\text{Mo}_2\text{Cl}_9$, 29013-05-6; $(\text{MeNH}_3)_3\text{Mo}_2\text{Cl}_9$, 22087-47-4; $(\text{EtNH}_3)_3\text{Mo}_2\text{Cl}_9$, 105132-60-3; $(\text{BuNH}_3)_3\text{Mo}_2\text{Cl}_9$, 105132-61-4; $(\text{HexNH}_3)_3\text{Mo}_2\text{Cl}_9$, 105132-62-5; $\text{K}_3\text{Mo}_2\text{Cl}_9$, 24355-00-8; $\text{Rb}_3\text{Mo}_2\text{Cl}_9$, 56376-82-0; $\text{Cs}_3\text{Mo}_2\text{Cl}_9$, 29013-02-3; $(\text{Me}_4\text{N})_3\text{Mo}_2\text{Cl}_9$, 24354-28-7; $(\text{Et}_4\text{N})_3\text{Mo}_2\text{Cl}_9$, 29013-04-5; $\text{K}_3\text{Mo}_2\text{Br}$, 111533-06-3; $\text{Rb}_3\text{Mo}_2\text{Br}$, 111533-07-4; $\text{Cs}_3\text{Mo}_2\text{Br}$, 29013-06-7; $(\text{Me}_4\text{N})_3\text{Mo}_2\text{Br}$, 111533-08-5; $(\text{Et}_4\text{N})_3\text{Mo}_2\text{Br}$, 29116-32-3; $\text{Cs}_2\text{Mo}_2\text{I}_9$, 105132-59-0; $(\text{Me}_2\text{NH}_2)_3\text{Mo}_2\text{Cl}_9$, 105132-63-6; $(\text{Et}_2\text{NH}_2)_3\text{Mo}_2\text{Cl}_9$, 105132-64-7; $(\text{Me}_3\text{NH})_3\text{Mo}_2\text{Cl}_9$, 105132-65-8; $(\text{Et}_3\text{NH})_3\text{Mo}_2\text{Cl}_9$, 33540-32-8; $(\text{PipeH})_3\text{Mo}_2\text{Cl}_9$, 39723-18-7; $(\text{PyH})_3\text{Mo}_2\text{Cl}_9$, 103727-40-8; $(\text{Et}_4\text{NH}_3)_3\text{Mo}_2\text{I}_9$, 119414-43-6.

Supplementary Material Available: Tables S1 and S2, containing observed and calculated peak intensities and the step-scan intensity data (22 pages). Ordering information is given on any current masthead page.